Tissue Eng Regen Med (2020) 17(4):537–552
https://doi.org/10.1007/s13770-020-00267-3

Online ISSN 2212-5469

ORIGINAL ARTICLE

The Therapeutic Potential of Extracellular Vesicles Versus Mesenchymal Stem Cells in Liver Damage

Dina M. Rostom[1] · Noha Attia[1,2] · Hoda M. Khalifa[1] · Maha W. Abou Nazel[1] · Eshrak A. El Sabaawy[1]

Received: 2 March 2020 / Revised: 5 April 2020 / Accepted: 15 April 2020 / Published online: 6 June 2020

Abstract

BACKGROUND: The extracellular vesicles (EVs) secreted by bone marrow-derived mesenchymal stem cells (MSCs) hold significant potential as a novel alternative to whole-cell therapy. We herein compare the therapeutic potential of BM-MSCs versus their EVs (MSC-EVs) in an experimental Carbon tetrachloride (CCl_4)-induced liver damage rat model.

METHODS: Rats with liver damage received a single IV injection of MSC-EVs, 1 million MSCs, or 3 million MSCs. The therapeutic efficacy of each treatment was assessed using liver histopathology, liver function tests and immunohistochemistry for liver fibrosis and hepatocellular injury.

RESULTS: Animals that received an injection of either MSCs-EVs or 3 million MSCs depicted significant regression of collagen deposition in the liver tissue and marked attenuation of hepatocellular damage, both structurally and functionally.

CONCLUSION: Similar to high doses of MSC-based therapy (3 million MSCs), MSC-EVs mitigated the fibrogenesis and hepatocellular injury in a rat model of CCl_4-induced liver fibrosis. The anti-fibrinogenic effect was induced by attenuating hepatic stellate cell activation. Therefore, the administration of MSC-EVs could be considered as a candidate cell-free therapeutic strategy for liver fibrosis and hepatocellular damage.

✉ Noha Attia
Noha.attia@alexmed.edu.eg

[1] Department of Medical Histology and Cell Biology, Faculty of Medicine, University of Alexandria, Dr. Fahmi Abdelmeguid St., Mowassah Campus, Alexandria 21561, Egypt

[2] Department of Basic Sciences, The American University of Antigua - College of Medicine, University Park, Jabberwock Beach Road, P.O. Box 1451, Coolidge, Antigua and Barbuda

Graphic Abstract

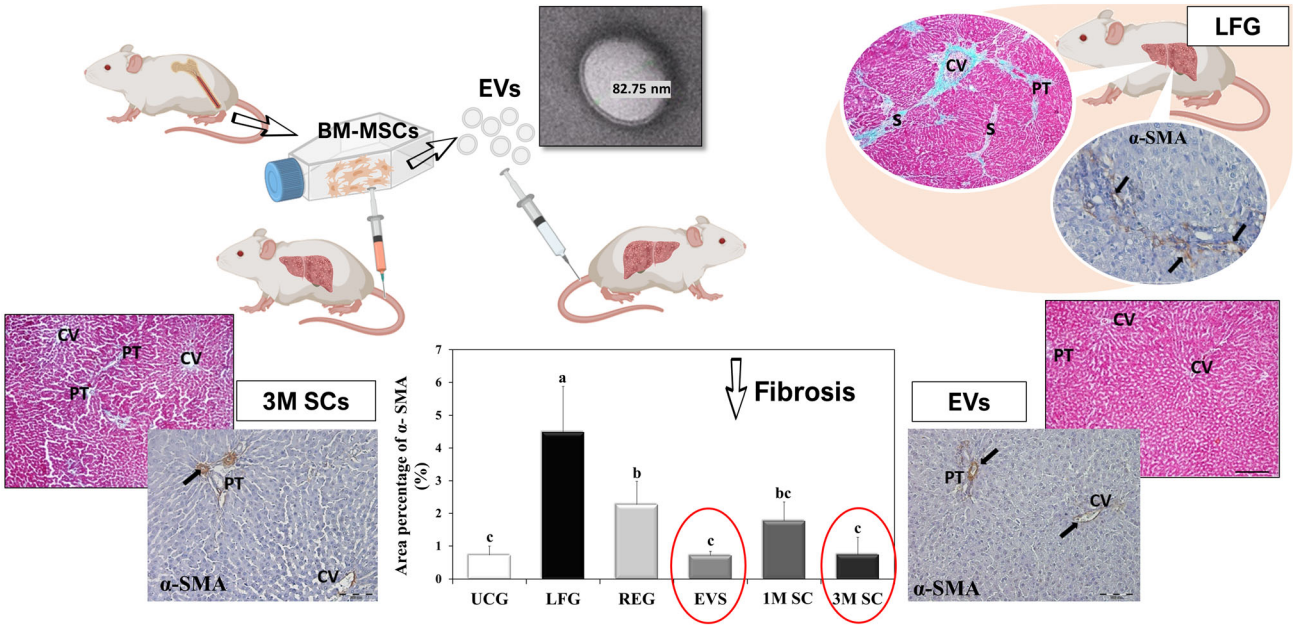

Keywords Extracellular vesicles · Exosomes · Bone marrow-derived stem cells · Liver fibrosis · Conditioned media

1 Introduction

Liver fibrosis comprises a worldwide health problem in industrialized countries in general. Cirrhosis, the end stage of fibrosis, is currently ranked as the 11th most common cause of death globally; accounting for approximately 1 million mortalities per year [1]. Furthermore, it is also a major risk factor for the development of hepatocellular carcinoma (HCC); more than 80% of HCCs develop on a fibrotic or cirrhotic background. The increased risk of HCC development associated with liver cirrhosis represents a significant healthcare issue, as HCC is the fifth most common solid tumor and the second leading cause of cancer-related deaths globally with a rising incidence in the United States of America and Europe [2].

Over the past two decades, clinical research has been working on determining the optimal therapeutic strategy for liver fibrosis. Liver transplantation is the only effective treatment for patients with end-stage liver diseases. Nevertheless, high cost, donor deficiency, long waiting lists, postoperative morbidity and mortality, and long-term side effects drastically limit its application [3]. Therefore, alternative therapies are being investigated to replace organ transplantation and overcome the obstacle for the lack of a timely available compatible graft.

Among the various types of stem cells, mesenchymal stromal cells (MSCs) have become a popular research topic as a result of their easy isolation, high expandability, multilineage differentiation potential, and paracrine activity all of which make them an ideal cell source for autologous stem-cell-based replacement therapies [4, 5]. MSCs can also be easily stored with minimal loss of potency and stored for point-of-care delivery [6].

Extensive research has been carried out to display MSCs' ability to restore damaged tissue in various organs including liver disease models, such as liver resection, acute hepatic failure, drug-induced liver injury, and cirrhosis. Nevertheless, the exact therapeutic mechanisms of MSCs in liver injury models are not clearly defined [7].

Extracellular vesicles (EVs) are released by almost all cell types, including stem cells, and serve an important role in intercellular communication [8]. They are classified into three types: microvesicles, exosomes and apoptotic bodies. EVs interact with target cells by surface-expressed ligands. EVs transfer surface receptors, deliver proteins, micro RNA (miRNA), and bioactive lipids [9].

Systemic administration of MSC-derived EVs has been proven to reduce myocardial infarct size in an acute myocardial infarction rat model [10]. MSC-EVs may exert a neuroprotective effect following stroke [11]. They have shown renal-protective effects in acute and chronic kidney disease [12], attenuated pulmonary inflammation in acute lung injury enhanced cutaneous regeneration [8], and promoted hepatic regeneration in drug-induced liver injury models [13]. Their positive effects have been attributed to their anti-inflammatory and anti-fibrotic effects, thus

suggesting that MSCs-EVs may serve as a novel therapeutic modality for diseases [8, 10, 11].

In this study, for the first time to the best of our knowledge, we compared the therapeutic potential of BM-MSCs versus their EVs in an experimental model of CCl_4-induced liver fibrosis in rats. Furthermore, we compared two different doses for BM-MSCs- based therapy, the low (1 million cells) and the high dose (3 million cells).

2 Materials and methods

2.1 Isolation, culture, and characterization of BM-MSCs

2.1.1 Isolation and culture of BM-MSCs

Three male Sprague-Dawley rats (3 weeks old—weighing 25–30 g) were euthanized, placed in a vertical laminar airflow hood where femurs were removed aseptically. The bone marrow cell suspension was obtained by flushing the marrow cavity using dispensable 3 ml syringe with complete culture media (CCM) composed of low glucose Dulbecco's modified Eagle's medium (LG-DMEM, Lonza, Basel, Switzerland) with the addition of 20% Fetal bovine serum (FBS, Hyclone, South America), 1% L-glutamine, and 1% penicillin/streptomycin (P/S 10,000 IU/ml and 10,000 µg/ml, respectively, Lonza, Switzerland). The bone marrow cell suspension was then filtrated through a 70 mm filter mesh and centrifuged at 1200 rpm for 5 min. The resulted cell pellets were resuspended in CCM and transferred into 25 cm^2 culture flasks and cultured at 37 °C under a humidified atmosphere containing 5% CO_2. After 48 h, the non-adherent cells were washed by phosphate-buffered saline (PBS) and CCM was changed twice weekly where the non-adherent/detached cells were removed. Once reaching ~ 70–80% confluency, adherent cells were detached using 0.25% trypsin-EDTA solution (BioWhittaker, Trypsin 1:250, EDTA 1 mM; Lonza) and re-seeded at 1:2 or 1:3 ratios. MSCs at passage four (P4) was utilized for subsequent experiments.

2.1.2 Characterization of BM-MSCs

Characterization of cell morphology and follow-up of cultured cells was done using a phase-contrast inverted microscope (Nikon TSM, Champigny-sur-Marne, France) equipped with a digital camera (DCM 510). Colony-forming unit-fibroblast (CFU-F) assay was performed; one hundred BM-MSCs were cultured in 10 ml of sterile CCM in a 100 mm diameter dish (about 55 cm^2 culture area). Cells were incubated for 14 days, with medium changes twice weekly. Then, the plate was stained with 3% Crystal Violet (Sigma-Aldrich, St. Louis, MO, USA) in 100% methanol to distinguish cell colonies.

Additionally, the phenotype of P4 MSCs' was authenticated using fluorescent-labeled monoclonal antibodies (mAb) for CD90 and CD45 surface markers. Cells were detached with 0.25% trypsin-EDTA solution, washed with PBS, and incubated (RT, 30 min, in the dark) with monoclonal Anti-CD90/Thy1 antibody (Allophycocyanin, Abcam, Cambridge, UK) and FITC-conjugated antibodies for CD45 (Abcam). The cells were subsequently washed three times with PBS, resuspended in 500 µL FACS buffer. Approximately 10^4 gated events were acquired and analyzed using a FACS Calibur flow cytometer running CellQuest software (Becton Dickinson, Sumter, SC, USA).

2.2 Isolation and characterization of MSCs-EVs

2.2.1 Isolation of MSCs-EVs

MSCs at P4 were allowed to grow to 80–90% confluence (~ 750,000 cells/T-75 cm^2 flask), then washed thoroughly (3 times) with PBS, and incubated in serum-free media (SFM) consisting of DMEM low glucose, supplemented with 1% L-glutamine and 1% P/S. After 24 h, the conditioned medium was collected and stored at − 80 °C. Subsequently, CCM was added to the flasks for another 24 h and the previous step was repeated.

EVs were isolated from the conditioned medium following the method of Gatti et al. [14], with some modifications. Briefly, the conditioned media was centrifuged at 2000 × *g* for 20 min to remove cells and debris. Cell/debris-free supernatant was filtered using a 0.22 µm syringe filter and then centrifuged at 110,000 × *g* for 70 min at 4 °C (Beckman Coulter Optima L-100 K ultracentrifuge, Fullerton, CA, USA).

2.2.2 Characterization of MSCs-EVs

To determine the morphology of MSCs-EVs, the suspension was loaded to copper grids, stained with 1% (w/v) phosphotungstic acid (PTA) and then examined by transmission electron microscopy (TEM) with an accelerating voltage of 120 kV (JEM-1400 series, Pleasanton, CA, USA) [15]. The size of MSCs-EVs was analyzed using the Zetasizer Nanoparticle analyzer (Malvern, UK).The protein content of MSCs-EVs was estimated by the Lowry protein assay (Bio-Rad laboratories, Richmond, CA, USA) according to the manufacturer's instructions.

2.3 *In vivo* study and experimental design

Thirty-six adult male Sprague-Dawley albino rats, weighing 150–200 g, were used at six to eight weeks of age.

Each rat had free access to both water and standard rodent soft chow ad libitum. In this study, rats were handled in strict accordance with the institutional guidelines for the care and use of laboratory animals. The protocol was approved by the institutional review board of animal experiments. The experimental rats were divided into two main groups (as illustrated in Fig. 1):

(i) Control groups (n = 18) including 3 subgroups:

1. Untreated Control Group (*UCG*) (n = 6) rats were left without treatment and sacrificed at week 13,
2. Liver Fibrosis Group (*LFG*) (n = 6). To induce liver fibrosis, rats were injected IP with Carbon tetrachloride (CCl_4, 99.5% purity, Chema tech, Tianjin, China) in olive oil (concentration 50%) at a dose of 1 µl/g body weight twice/week for 9 successive weeks and were sacrificed at week 9. Each rat was weighed once weekly to adjust the dose.
3. Regression group (*REG*) (n = 6) rats were observed for spontaneous regression of fibrosis for an additional 4 weeks. Each rat received a single IV injection of PBS via the tail vein and sacrificed at week 13.

(ii) Treatment groups (n = 18), 24 h after the last CCl_4 injection, each rat received a single IV injection (via the tail vein) of either:

1. 80 µg EVs protein/rat in 1 ml PBS, (*EVS*) *Group* (n = 6),
2. 1×10^6 MSCs in 1 ml PBS, (*1M SC*) *Group* (n = 6),
3. 3×10^6 MSCs in 1 ml PBS, (*3M SC*) *Group* (n = 6).

All treatment groups were sacrificed 4 weeks post-injection.

2.4 Biochemical study

Before rats were euthanized, blood samples were collected from the inferior vena cava in plain tube vacutainers and left for 30 min to clot. The serum was isolated within 1 h by centrifugation at 2000×*g* for 10 min. Sera from all groups were stored at − 80 °C then an Automated Chemical Analyzer (7600; Hitachi, Tokyo, Japan) was used to estimate the serum enzymes aspartate transaminase (AST) and alanine transaminase ALT (µ/l) and albumin (g/dl) according to the manufacturers' instructions.

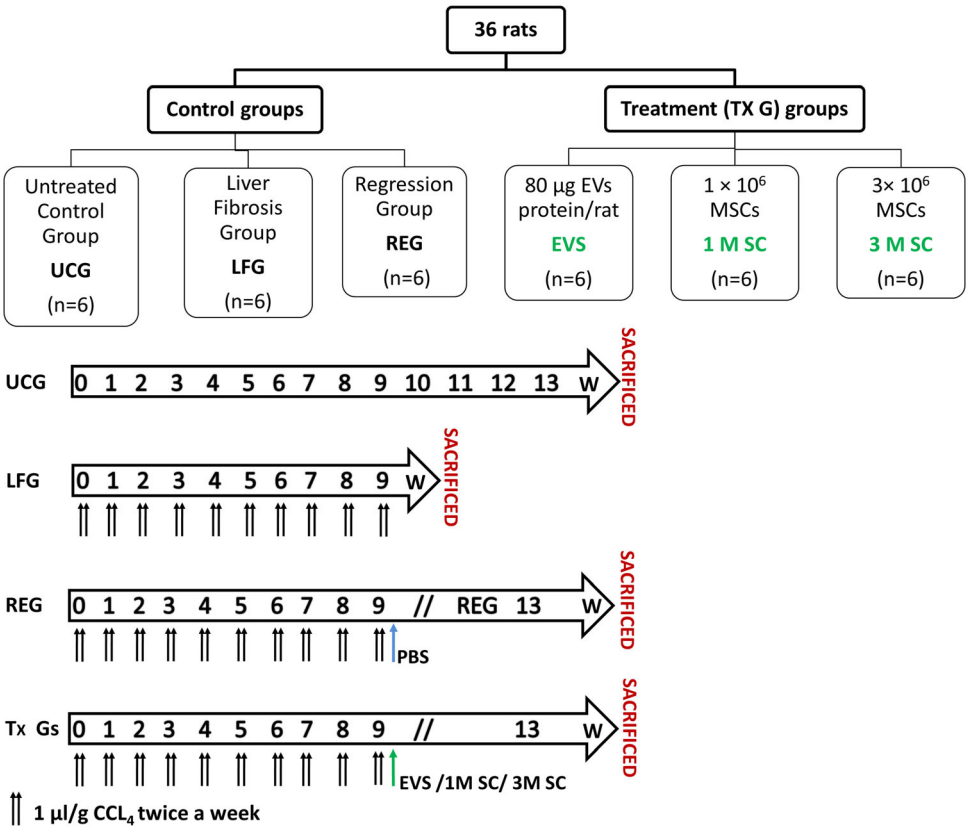

Fig. 1 Diagrams depicting the experimental design for the study

2.5 Histological and immunohistochemical study

The right lobe of the liver of all specimens was fixed in 10% buffered formalin, embedded in paraffin, and sectioned into 5 μm thick sections.

2.5.1 Histological study

Sections were de-paraffinized and stained with hematoxylin and eosin (H&E) and Gomori's trichrome stains. Histological assessment was performed by a blinded observer, who scored the liver sections to assess hepatocellular death and inflammation using the following criteria Normal histology "0"; minor hepatocellular death and inflammation "1"; widely distributed patchy necrosis and inflammation "2"; complete disruption with panlobular necrosis and inflammation "3"; mortality "4". To assess liver fibrosis, the scoring system of Ishak et al. [16] was used where 0 = no fibrosis, 1 = expansion of some portal areas with/without septa, 2 = expansion of most portal areas with/without septa, 3 = expansion of most portal areas with portal-portal bridging, 4 = expansion of most portal areas with portal-portal and portal-central bridging, 5 = bridging with occasional nodules, 6 = cirrhosis probable or definite.

The histomorphometric analysis was performed using the NIH Fiji© program (Wayne Rasband, MD, USA). Images were captured for Gomori's trichrome-stained sections with a Digital camera (Olympus DP20) connected to the microscope (Olympus BX41) at a microscopic magnification of × 100. The area percentage of collagen density was measured in random sections. Data were presented as mean ± SD (n = 6/group).

2.5.2 Immunohistochemistry

Liver tissue sections were obtained and mounted to positively charged slides. The immune-staining procedure was done following the streptavidin–biotin-immunological detection of α smooth muscle actin (α-SMA) protocol according to the manufacturer's protocol. The primary antibodies anti-smooth muscle actin (Mouse monoclonal antibody, Thermo, diluted at 1:800) as well as the detection system kit (UltraVision detection system, Thermoscientific, Fremont, CA, USA) was purchased from Lab Vision Corporation (Thermo Fisher, Fremont, USA). All reactions were performed using appropriate positive and negative controls. Finally, slides were counter-stained with hematoxylin. Digital images were obtained from the immunohistochemically stained sections using a Digital camera (Olympus DP20) connected to the microscope (Olympus BX41) at magnification × 100. Measurements were expressed in the form of a percentage area using the NIH Fiji© program (NIH, USA). Data were presented as mean ± SD (n = 6/group).

2.6 Statistical analysis

The biochemical and morphometric results were analyzed using IBM SPSS software package version 20.0. (Armonk, NY: IBM Corp). Kolmogorov–Smirnov test was used to verify the normality of distribution. Quantitative data were expressed as mean ± standard deviation (SD). Significant differences were determined using ANOVA and pairwise comparison (between each 2 groups) was done using the Post Hoc Test (Tukey). Values were considered significant when $p < 0.05$.

3 Results

3.1 Morphologic and immunophenotypic characterization of BM-MSCs

Two to three days after seeding, spindle-shaped plastic adherent cells were detected. Adherent cells continued to proliferate and reached a confluence of 70–90% on day 15. When examined with an inverted phase-contrast microscope, the primary cells were adherent, fusiform or polygonal in shape with multiple small cytoplasmic projections. Cultures of P0–P4 were photographed when they were almost semi confluent, denoting that cellular morphology and proliferative potential were maintained in the passages adopted in this study (Fig. 2A for P0 and 2B for P4). The CFU-F assays demonstrated that the cultured cells contained a subpopulation capable of generating new multiple fibroblast-like colonies from single cells (Fig. 2C). The FACs analysis of P4 cells demonstrated that almost 91.65% of cultured cells expressed the stemness marker CD90, albeit 99.74 depicted the absence of hematopoietic marker CD45 (Fig. 2D).

3.2 Characterization of BM-MSCs-EVs

MSCs-EVs were isolated from rat bone marrow-derived MSCs *in vitro* by using an ultracentrifugation-based protocol. When examined by the TEM, MSCs-EVs appeared as double membrane-bound spheroid vesicles of variable sizes (Fig. 3A). The isolated vesicles had a mean size of 113.7 as measured by Zetasizer (Fig. 3B). The total protein content of the EVs suspension using the Lowry method was estimated to be. 15.49 μg ± 0.6/1 × 10^6 BM-MSCs cultured in serum-free media for 24 h.

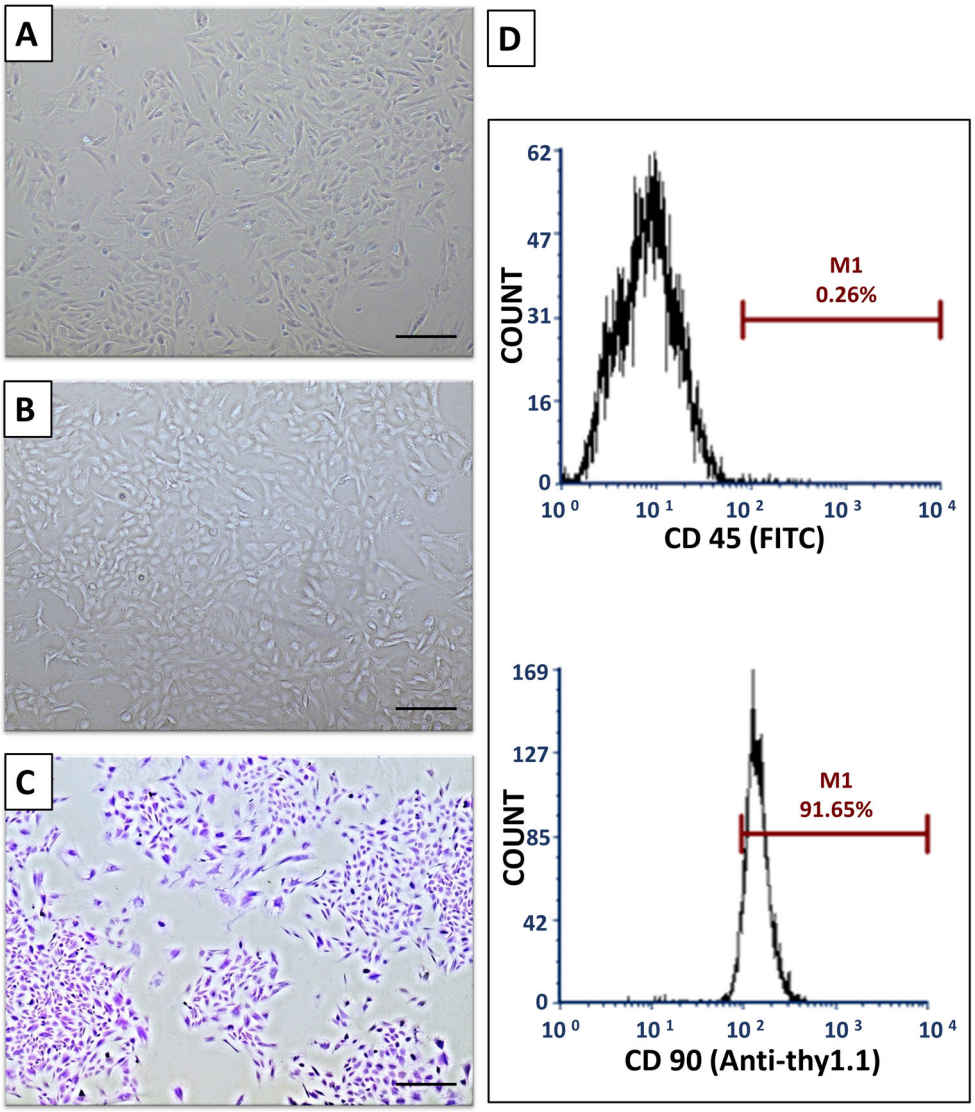

Fig. 2 Characterization of BM-MSCs. **A** Passage zero (P0) cells. **B** Passage four cells P4. **C** Crystal violet-stained colonies. (Phase contrast microscope, Original magnification × 100) **D** A representative flow cytometric analysis of cell-surface markers of BM-MSCs at P4

3.3 Histological, morphometric and biochemical results

3.3.1 Histological examination of H&E staining

Histological examination of H&E-stained liver sections of the control group that received no treatment (UCG) revealed normal hepatic architecture with average stroma and structural components in the portal tracts. The hepatocytes were polyhedral in shape with granular acidophilic cytoplasm and rounded vesicular centrally located nuclei, some cells were binucleated (green arrows). In between the hepatic cords, the hepatic sinusoids(s) appeared as narrow spaces lined by flattened endothelial cells (arrows) and few bulging Kupffer cells (arrowheads). The portal tracts (PT) were seen at the periphery of hepatic lobules (Fig. 4A, B). Following CCl_4 treatment, the LF group (LFG) exhibited disorganized hepatic architecture with numerous connective tissue septa connecting adjacent portal areas (PT) (Porto-portal fibrosis) (arrows) with the formation of pseudo lobules. Hepatocytes displayed variable degrees of centrilobular degenerative changes, involving wide-spread segments of several hepatic lobules and individual apoptotic cells. Many individual hepatocytes were vacuolated while others were shrunken with hypereosinophilic hyalinized cytoplasm (acidophilic bodies) (red arrows). Nuclear changes included pyknosis and karyolysis (arrowheads). Pronounced signs of hepatic inflammation were depicted in the form of mononuclear cellular infiltration (I), mainly in the portal areas and in newly formed connective tissue septa. Most of the blood sinusoids (s) between the affected hepatic cords displayed widening. The portal area revealed evident proliferation of bile ducts (asterisks) (Fig. 4C, D). According to the blinded observer the degree

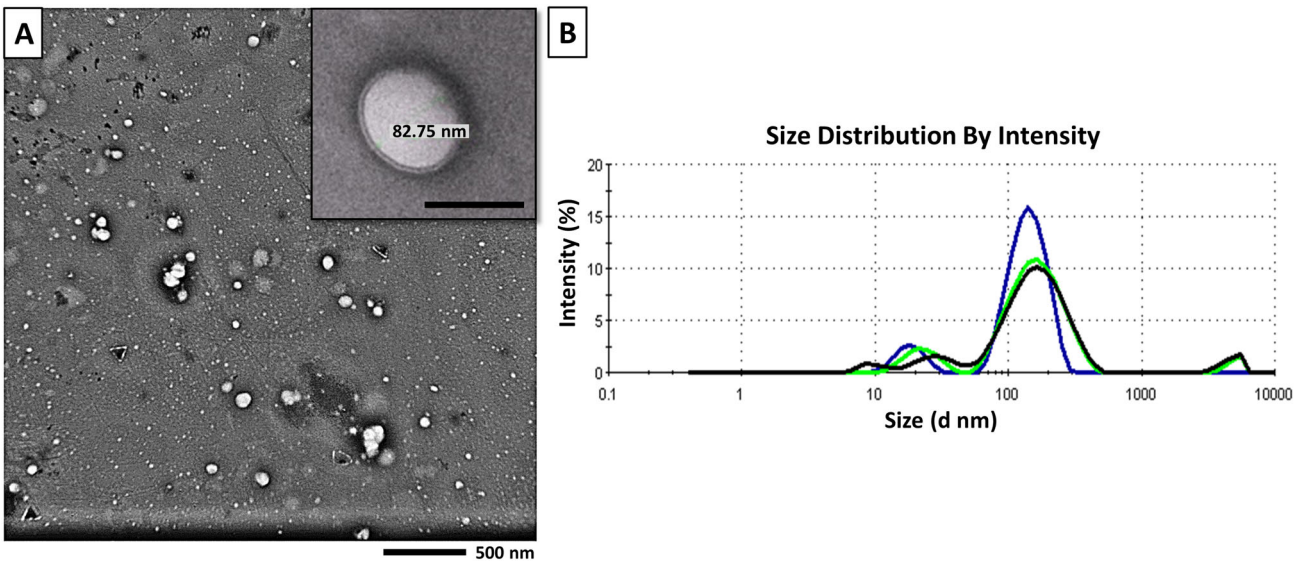

Fig. 3 Characterization of MSCs-EVs. **A** Morphology of EVs by Transmission electron microscope (TEM) (Magnification × 4.000, Scale Bar: 500 nm). Inset: Magnification × 10,000, Scale bar: 100 nm. **B** The size distribution of EVs by Zeta sizer

of hepatocellular death, inflammation was assessed (Score: 3) (Table 1). Meanwhile, in the group observed for spontaneous regression of fibrosis for an additional 4 weeks; the regression group (REG) the liver was still markedly affected (Fig. 4E, F) (hepatocellular death and inflammation score: 3) (Table 1). Increased connective tissue fiber deposition was observed in portal areas leading to their expansion (black arrows), forming septa connecting adjacent portal tracts (red arrow) and around the central veins (green arrow). Panlobular necrosis (N) was also depicted; hepatocytes appeared shrunken with deeply stained acidophilic cytoplasm and pyknotic nuclei. Obliteration of sinusoids (s) and proliferated bile ducts (asterisks) was also seen.

When compared to the LFG, all treatment groups exhibited improvement but to various extents. Rats that received either EVs (EVS) or 3×10^6 MSC (3M SC) revealed remarkable improvement of the previously described histopathological lesions (hepatocellular death and inflammation score: 1) (Table 1). Hepatocytes formed one or 2 cell thick cords radiating from central veins and separated by blood sinusoids. Most hepatocytes appeared large, polyhedral, with granular acidophilic cytoplasm and large central vesicular nucleus with prominent nucleoli. A few cells appeared with deeply stained cytoplasm and small dark nuclei (arrowheads). Signs of liver regeneration including increased cell plate thickness (double-headed arrows), increased number of binucleated cells (green arrows) and mitotic figures (m) were depicted in both groups (Fig. 5A, B and E, F respectively). Whereas rats that received 1×10^6 MSCs (1M SC) demonstrated the persistence of some of the CCl_4 hepatic lesions (Fig. 5C, D) (hepatocellular death and inflammation score: 2) (Table 1).

After 9 weeks of CCl_4 treatment, ALT and AST enzymes were significantly increased in the LFG compared to UCG ($p \leq 0.001$). All treatment groups (EVS, 1M SC, and 3M SC) depicted significantly reduced levels of ALT and AST in sera of rats and showed no significant difference ($p \leq 0.05$) when compared to the UCG. As for the REG group a significant increase ($p \leq 0.001$) in the levels of ALT and AST persisted in comparison to the UCG and revealed no significant difference to the LFG ($p \leq 0.05$). There was also a significant decrease in the mean value of serum albumin levels in the LFG and REG groups ($p \leq 0.001$) as compared to the UCG. The serum albumin levels were recovered to control levels in the MSCs-treated groups (1M SC & 3M SC), but not in the EVS group (Fig. 5G–I).

3.3.2 Gomori's trichrome staining

The Gomori's trichrome-stained sections of UCG appeared to be supported with stroma of very delicate meshwork of collagenous fibers. Few collagen fibers were seen surrounding central veins and portal areas (Fig. 6A). Rats of the LFG, REG and 1M SC groups developed a significant increase in collagen deposition (fibrosis) as compared to UCG ($p \leq 0.001$) (Ishak score: F3, F2–F3, F2 respectively). In the LFG, increased collagen deposition was seen around central veins, portal tracts, in between hepatocytes, forming fibrous tissue septa and pseudo-lobules (Fig. 6B). The REG group revealed the persistence of intense collagen staining similar to that of the LF group ($p \leq 0.05$)

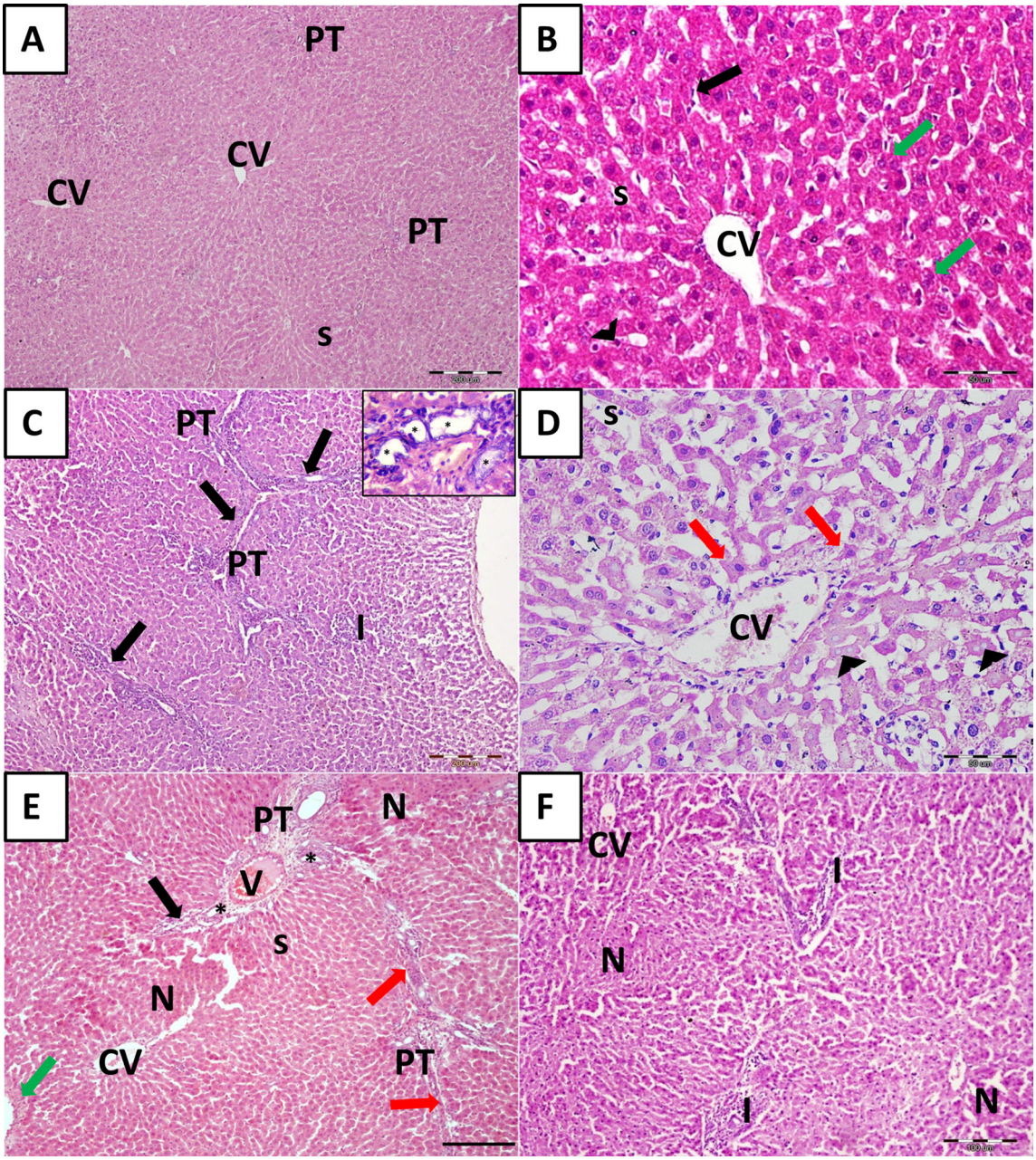

Fig. 4 Histological assessment of the liver tissue of CCl_4-treated animals. **A**, **B** Binucleated hepatocytes (green arrows). Sinusoids (s) are lined by endothelial cells (arrows) and Kupffer cells (arrowheads). **C** Liver fibrosis group (LFG). Fibrous tissue septa (arrows), mononuclear cellular infiltration (I). Inset: proliferated bile ducts (asterisks). **D** Liver fibrosis group (LFG). Hypereosinophilic hepatocytes (red arrows) and loss of nuclei (arrowheads). **E**, **F** Regression group (REG). Expansion of portal areas (black arrows), Porto-portal connective tissue septa (red arrow) and increased connective tissue deposition around central veins (green arrow). Note, the areas of hepatic necrosis (N), proliferated bile ducts (asterisks), sinusoids (s), cellular infiltration (I), portal tract (PT);central vein (CV). [H&E scale bar (**A**, **C**, **E**) 200 μm (**B**, **D**) 50 μm, and (F) 100 μm]

(Fig. 6C). The collagen deposits in rats that received 1M SC displayed sporadic, small fibrotic lesions in the peri-portal zones. The amount of collagen deposition was similar to that seen in both the LFG and REG group ($p \leq 0.05$) (Fig. 6E). In rats treated with EVs and 3M SC collagen fiber distribution around central veins and portal tracts were comparable to that of the control group ($p \leq 0.05$) (Fig. 6D, F, respectively) (Ishak score: F0). The results were statistically confirmed by values obtained from morphometric analysis (Fig. 6G).

Table 1 Assessment of hepatocellular death and inflammation score (scores from 0 to 4) and degree of fibrosis using Ishak et al. scoring system (0–6)

Group	Hepatocellular death score	Ishak grade: categorical assignment
UCG	0	F0
LFG	3	F3
REG	3	F2-F3
EVS	1	F0
1M SC	2	F2
3M SC	1	F0

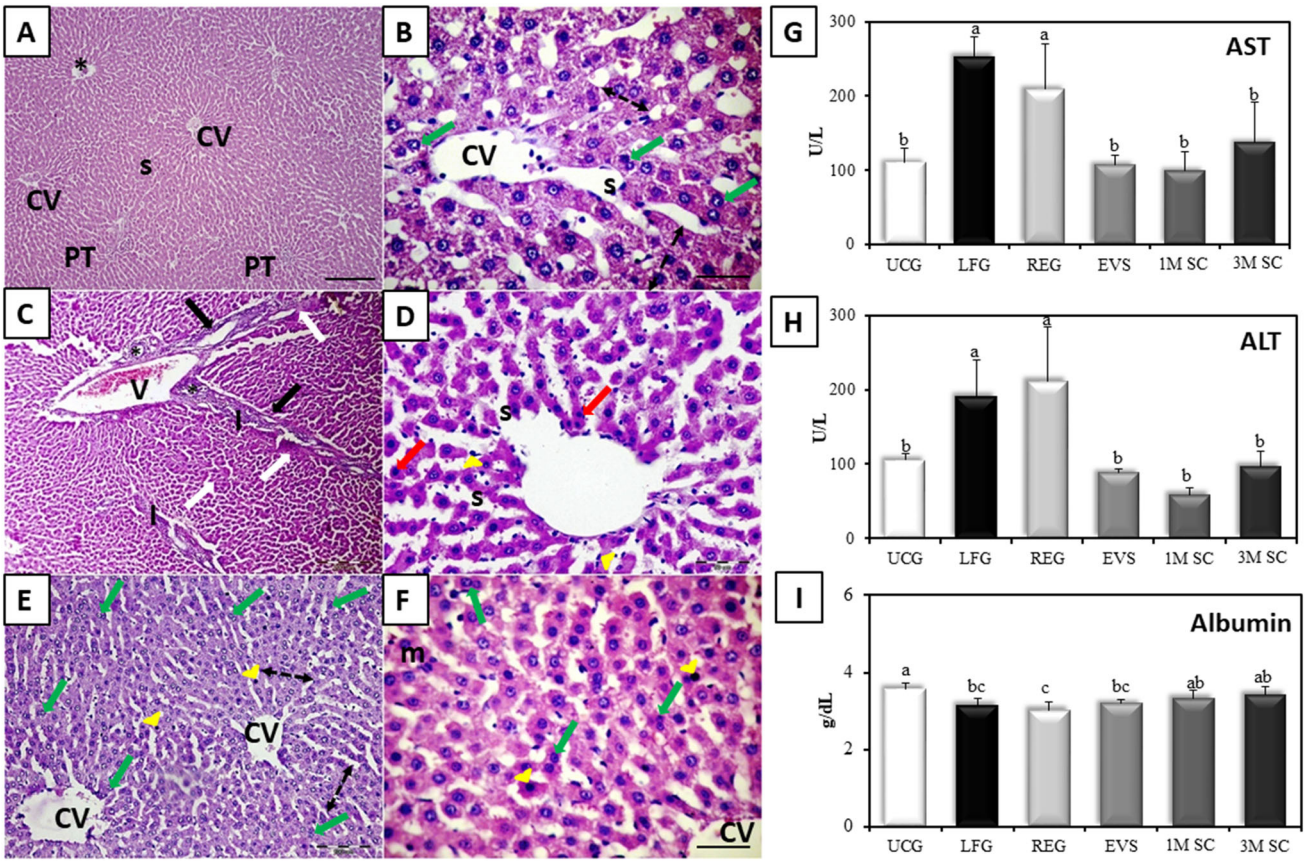

Fig. 5 Impact of MSCs and EVs CCl_4-induced liver fibrosis. **A**, **B** Liver tissue of EVs-treated group following induction of liver fibrosis (EVS). Binucleated hepatocytes (green arrows) S; dilated sinusoids.CV; central vein. H&E. Scale bars (**A**) 200 µm, (**B**) 50 µm. **C**, **D** Liver tissue of the 1M SC group. Portal vein (V), proliferated bile ducts (asterisks), periportal fibrous septa (arrows) with areas of periportal mononuclear cellular infiltration (I) and sporadic necrosis (red arrows), pyknotic nuclei (white arrows) dilated sinusoids (s) and proliferation of Kupffer cells (arrowheads). [H&E Scale bars (**C**) 200 µm, (**D**) 50 µm]. **E**, **F** The liver of rats that received 3×10^6 MSCs (3M SC) increased cell plate thickness (double-headed arrows) and mitotic figure (m) in (**F**). Note, the few sporadic apoptotic cells (arrowheads). central vein (CV) [H&E Scale bars (**E**) 200 µm, (**F**) 50 µm]. **G**, **H** Serum AST and ALT levels (U/L) **I** Serum albumin levels (g/dL). Values represent mean ± SD (n = 6). Statistical significance was determined using ANOVA test, Pairwise comparison between each 2 groups was done using Post Hoc Test (Tukey). Similar letters indicate no statistical difference ($p > 0.05$), while different letters would indicate a true statistical difference ($p < 0.05$)

3.4 Immunohistochemistry

Immunohistochemical evaluation of an α-SMA expression in UCG showed mildly immunoreacted α-SMA positive cells around the wall of central veins and blood vessels of portal tracts while other liver cells remained negative (Fig. 7A). The LFG showed a significant increase ($p \leq 0.001$) in immune-reacted α-SMA positive cells when compared to the UCG. These cells were detected in-between the hepatocytes, as well as in the connective tissue septa between the hepatic lobules. At high magnification, they appeared as small spindle-shaped cell bodies with an intense positive brownish cytoplasmic reaction and multiple cytoplasmic processes connected to one another

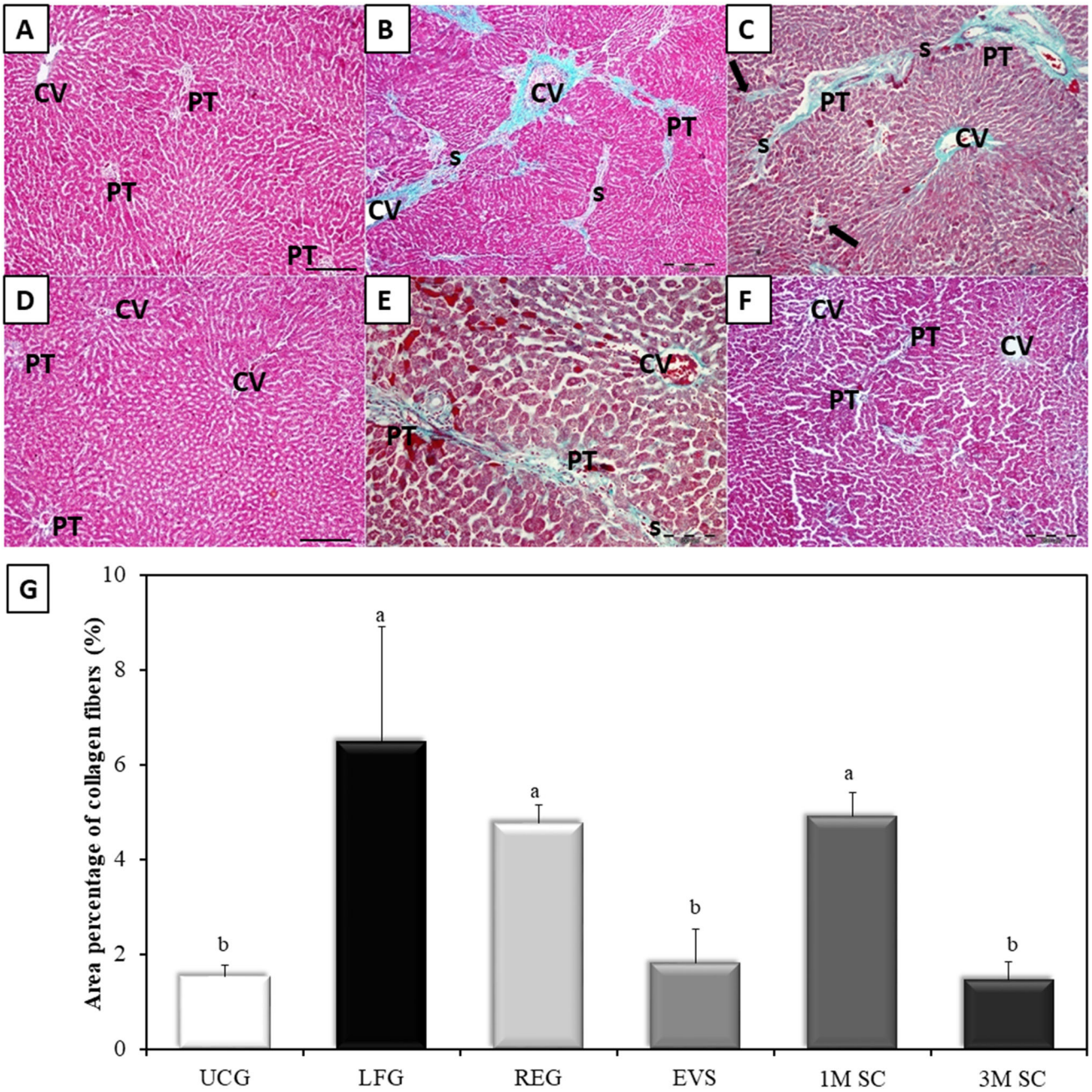

Fig. 6 Collagen distribution in the liver tissue by Gomori's trichrome stain. Collagen fibers are stained in green. **A** Control rat liver (UCG), **B** Liver fibrosis group (LFG). **C** Liver of rats in the REG group. The collagen fiber distribution of (EVS) in (**D**), that of 3M SC in (**F**), and 1M SC in (**E**). Central veins (CV), portal tracts (PT), fibrous septa (S), necrotic hepatocytes (arrows). Scale bars 200 µm, except for **E**, scale bar 100 µm. **G** Area percentage of collagen fibers (%): Values represent mean ± SD (n = 6). Statistical significance was determined using ANOVA test, Pairwise comparison between each 2 groups was done using Post Hoc Test (Tukey). Similar letters indicate no statistical difference ($p > 0.05$), while different letters would indicate a true statistical difference ($p < 0.05$)

(Fig. 7B). The α-SMA-positive cells were significantly reduced in the REG group and all 3 treatment groups when compared to the LFG ($p \leq 0.001$). The REG group revealed clusters of moderately α-SMA-positive cells (Fig. 7C). In the liver of rats of the 1M SC group, α-SMA immunopositivity was still seen around portal tracts and extending outside the vessels (Fig. 7E). The livers of rats treated with either EVS or 3M SC showed a staining pattern similar to control animals ($p \leq 0.05$) (Fig. 7D, F, respectively). The results were statistically confirmed by values obtained from morphometric analysis (Fig. 7G).

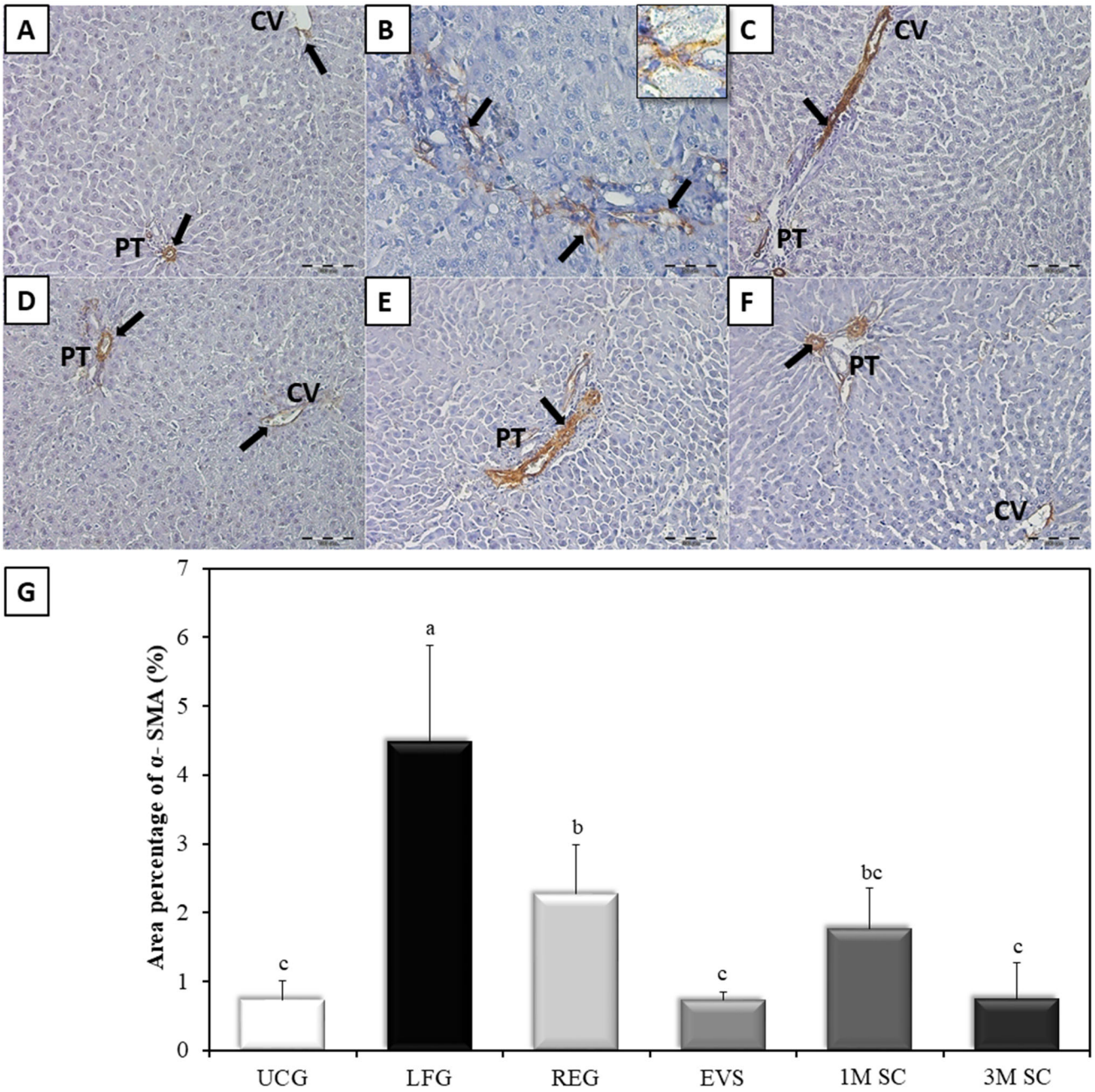

Fig. 7 Specific distribution of α-SMA in the liver tissue. **A** Control animals (UCG). **B** Rats of LFG. Inset: α-SMA positive cell at magnification × 1000 appears spindle in shape with multiple cytoplasmic processes. **C** The regression group (REG). The livers of rats receiving EVs and 3 × 10^6 MSCs (3M SC) (**D**, **F** respectively). The livers of rats that received 1 × 10^6 MSCs (1M SC) (**E**). Central veins (CV), portal tracts (PT). Immunopositive areas of α-SMA. (arrows). Scale bars of **A**, **C**, **D**, **E**, and **F** 100 μm. Scale bar of **B** 50 μm. **G** Area percentage of α-SMA (%): Values represent mean ± SD (n = 6). Statistical significance was determined using ANOVA test, Pairwise comparison between each 2 groups was done using Post Hoc Test (Tukey). Similar letters indicate no statistical difference ($p > 0.05$), while different letters would indicate a true statistical difference ($p < 0.05$)

4 Discussion

In the current work, Sprague-Dawley rats were used for the isolation of BMSCs [17]. When deciding on a dose for BM-MSCs literature review demonstrated doses as low as 1 million MSCs [18] others as high as 3 million MSCs [19] so it was decided to use both doses and compare them to the therapeutic effect of BM-EVs. Regarding the administration route, MSC transplant was performed by intravenous injection via the tail vein, the most commonly used and convenient mode of MSC transplantation [19] that has

shown clinical efficacy in several preclinical models and preliminary clinical settings [20].

Cells depicted fibroblast-like morphology and grew into colonies. The efficiency with which they form colonies remains an important assay for the quality of cell preparations [21]. These colonies started to appear on day 5–7 post-seeding and continued to proliferate rapidly onwards reaching 80–90% confluency at 12–14 days. Typically, the cultured cells were collected at this point of confluency to prevent contact inhibition of growth and spontaneous differentiation [22].

To further characterize BM-MSCs immunophenotyping of P4 BM-MSCs demonstrated that the majority of them expressed the stemness marker CD90, albeit depicted the absence of hematopoietic marker antibodies CD45, indicating the relative purity of the cultured MSCs [23].

The first step of extraction of extracellular vesicles was harvesting the cell culture supernatant (conditioned media; CM). The CM was obtained from P4 BM-MSCs (similar to those used for systemic infusion) to allow fair comparison. MSCs at 70–80% confluence were utilized as contact inhibition may decrease EVs secretion and/or alter their characteristics compared to those produced by actively dividing cells [24]. The obtained CM was stored at − 80 °C which is a favorable condition for the preservation of fresh exosomes for pre-clinical and clinical applications [25].

In the current experiment, EVs were isolated from CM following the method of Gatti's [14] ultracentrifugation-based protocol, yet with some modifications. Following the low-speed centrifugation ($2000\times g$ for 20 min), the first step of ultracentrifugation was replaced with a single filtration step using a 0.22-μm filter thus eliminating dead cells and large debris while keeping vesicles for further purification by ultracentrifugation. Also, the washing step was skipped as it was considered of no significant impact on the protein yield [26]. Altogether, we believe that the current protocol is easier, less time consuming and more cost-effective. In addition, the protein equivalent of EVs per 1 million cells (15.49 ± 0.6 μg) was markedly higher than the mean value obtained previously by ultracentrifugation protocols (3.07 μg) [26, 27].

Upon reviewing literature, there was great discrepancy in the doses of EVs used. Doses as low as 0.4 μg and others as high as 250 mg were used in different disease models [28]. In the current experiment, each rat in EVS group was injected with EVs equivalent to 80 μg of protein. Similar doses were previously reported to reduce fibrosis, have anti-inflammatory effects and promote angiogenesis in myocardial infarction [29, 30], improve survival in a lethal model of acute kidney injury [12] and promote neurovascular remodeling and functional recovery after stroke in rats [31].

EVs released by a single cell type can be classified based on their biogenesis into three major subtypes: exosomes, microvesicles and apoptotic bodies. Due to a significant overlapping in size, similarities in composition and absence of specific markers, it is very difficult to allocate individual EVs to one of the biogenesis pathways. In order to avoid any confusion about the nomenclature, it has been suggested by the ISEV community in the recently updated position paper on the Minimal Information for Studies of Extracellular Vesicles (MISEV2018), to use the term "extracellular vesicle (EV)" unless the subcellular origin of the vesicle is demonstrated [32]. Within this context, the protocol used was designed to separate exosomes fraction from the CM. As well, particle analysis revealed that most vesicles were below 120 nm (size of exosomes). Nevertheless, the term EVs was adopted in the current work because it does not discriminate between the different subsets of vesicles isolated.

The light microscopic examination of the liver of LFG rats revealed a loss of the usual hepatic architecture and hepatocyte injury (hepatocellular death and inflammation score: 3) which might be due to increased membrane permeability as a result of peroxidation of lipid membranes by the ROS generated after CCl_4 intoxication. The altered cell membrane permeability may also explain the significant increase in serum AST and ALT observed in the LFG when compared to the UCG [33]. Moreover, hepatocyte necrosis was seen mainly around the centrilobular region (acinar zone 3) which is a common site for drug-induced necrosis. Necrosis, in general, is characterized by increased eosinophilia due to loss of the normal RNA-induced basophilia and increased binding of eosin to denatured intracytoplasmic proteins [34]. This CCl_4-induced hepatocyte damage was reflected on the significant decrease in serum albumin levels in the LFG, thus indicating a perturbed synthetic ability of the liver [35].

The nuclear changes observed in the LFG which included pyknosis, and karyolysis, could be due to nonspecific breakdown of DNA by free radicals produced during the biotransformation of CCl_4 and activation of DNase activity respectively [34].

Based on both experimental and clinical studies there is a growing body of evidence that suggests that hepatocyte apoptosis may contribute to liver fibrogenesis. The hypothesis relating hepatocyte apoptosis to fibrosis suggests that apoptotic bodies are phagocytosed by Kupffer cells, hepatic stellate cells (HSCs) and adjacent hepatocytes which results in the production of chemokines and cytokines, including TGF-β1, which in turn activates HSCs leading to fibrosis [36, 37].

The sinusoidal dilation noticed maybe secondary to portal outflow obstruction (veno-occlusive lesion) or as a result of a nonspecific inflammatory response to CCl_4.

Activation of the interleukin-6 and vascular endothelial growth factor-related pathways are thought to play a role in sinusoidal dilatation [38]. Increased number of hypertrophied Kupffer cells is supposed to be implicated as a critical mediator of the inflammatory and fibrogenic responses during CCl_4-mediated liver insult [39].

Bile duct hyperplasia/proliferation seen in many portal areas of the LFG is part of a ductular reaction to liver insult [40]. Toxic liver injury is usually associated with augmented biliary secretion as a mechanism for eliminating the detoxification metabolites. Subsequently, the proliferation and elongation of biliary ductules occur to enhance the drainage of excess bile [41].

On the other side, in both the EVS and 3M SC groups, the liver fibrosis seems to be resolved following treatment (hepatocellular death and inflammation score: 1). The widespread double-cell plates, increased cell plate thickness, increased number of binucleated cells and mitotic figures are signs of increased hepatocyte proliferation and liver regeneration seen in both groups [42]. In contrast, the low dose of 1 million MSC (1M SC) group displayed limited improvement of the hepatocellular damage and inflammation (hepatocellular death and inflammation score: 2). with the persistent expansion of some portal areas and a few septa formation.

A critical step in any new therapeutic agent development is the establishment of its optimal dosage. This can be particularly challenging when using biologic agents that might exert their therapeutic effects via complicated or poorly understood mechanisms. Although it might seem logical to expect that the observed outcome would be directly proportionate to the number of cells administered. Conversely, some studies using MSCs in the treatment of acute myocardial infarction have shown inverse dose-response effects [43] or no dose-dependent effect [44]. In our study, the BM-MSCs dose was reflected in the degree of tissue restoration. Yet, being dose-dependent/ dose-independent still needs further work to verify the potential of a wider range of doses.

In parallel to the improvement of the histopathological structure of liver tissue confirming the therapeutic effect in EVS and 3M SC groups, the liver biomarkers -ALT and AST serum levels- were significantly recovered and returned to the control values in agreement with similar previous studies [34, 35]. On the other hand, serum albumin levels did not reach control levels in the EVS group. Lagging functional recovery, particularly in synthetic capacity suggests that protein synthesis was utilized for the constitution of liver parenchyma rather than excretion of albumin and would have probably improved later on [45].

In this research, liver fibrosis was clearly demonstrated by a significant increase in area percentage of collagen fibers (Ishak score: F3) and α-SMA positive cells in the LFG. Deposition of collagen results mainly from the activation of HSCs, the primary cell type that mediates fibrogenesis.

Under normal conditions (UCG), HSCs are non-parenchymal quiescent cells for vitamin A storage. However, in pathological conditions as in liver fibrosis, HSCs are activated by ROS and cytokines released from damaged hepatocytes and activated Kupffer cells. These activated HSCs lose retinoid, change to myofibroblasts-like cells and synthesize a large amount of extracellular matrix (which includes collagen, proteoglycan, and adhesive glycoproteins) [2, 46]. The α-SMA has long been described as a good marker for the detection of these myofibroblasts-like cells and is considered as a key biomarker for liver fibrosis [47, 48].

In the REG group, the persistence of the intense collagen staining similar to that of the LFG was observed (Ishak score: F3), these findings are in accordance with previous studies [33]. On the other hand, the number of HSCs was significantly reduced.

There is clear evidence in the literature that mild to moderate fibrosis is reversible when the stimuli responsible for chronic or repeated hepatic inflammation are successfully removed. Once extensive crosslinks develop in collagen (cannot be degraded by collagenase enzyme), the fibrous scar becomes very stable, and the body has no way to degrade it [49]. During the resolution of hepatic fibrosis, the activated HSCs can be cleared by apoptosis or reversion to their inactivated phenotype leading to degradation of the ECM [46]. These findings suggest that fibrosis has reached an irreversible stage or resolution might need more time to take place.

The resolved liver fibrosis seen in both the EVS and 3M SC groups (Ishak score: F0) was in accordance with the reduction of α-SMA-positive cells. On the other hand, significant fibrosis was still seen in the 1M SC group (Ishak score: F2). While the area percentage of α-SMA positive cells were significantly decreased.

The therapeutic potential of MSCs is mediated mostly via paracrine mechanisms rather than trans-differentiation [4, 8]. The paracrine mechanism includes secretion of (1) soluble factors and (2) the transfer of exosomes/microvesicles packed with various molecules including proteins (most of which are growth factors, cytokines, and chemokines), mRNAs, genes and miRNAs [50]. Therefore, the therapeutic effect of EVs mimicked the beneficial effects of 3 × 106 MSCs administration and was better than that of the 1 × 106 MSCs especially that the 80 μg of EVs protein, in our experiments, were secreted from approximately 5 million MSCs.

BM-MSCs ameliorated liver fibrosis most probably by an integrated set of mechanistic actions including the regulation of profibrotic and antifibrotic hepatic genes and

induction of HSCs apoptosis and inhibiting its activation, to mention a few [3, 4, 35, 51, 52].

The attenuated inflammatory response seen in both the 3M SC and the EVS group could be explained by local down-regulation of pro-inflammatory cytokines and up-regulation of anti-inflammatory cytokines such as IL-10 and has been described in several models including lung, kidney and heart injuries [53].

Upon liver insult, the body attempts to repair the damage through increasing HGF, TGF-β and other cytokines expression to enhance hepatocyte proliferation and initiate tissue repairing process. It was found that BM-MSCs secrete a variety of these cytokines and growth factors that enhance angiogenesis and stimulate mitosis and differentiation of tissue-intrinsic stem cells and hence promote liver regeneration. Our results demonstrate that MSC therapy can increase the number of proliferating hepatocytes in the regenerating, injured liver and that EVs are sufficient to accomplish this effect. This might be reflected by an apparent increased number of binucleated hepatocytes, increased cell plate thickness and mitotic figures observed in liver sections of both EVS and 3M SC group [54].

Similarly, several EVs-associated factors have a well-known antiapoptotic and liver regeneration–stimulating effect [8, 10]. These factors do not only reduce the inflammation, apoptosis, and fibrosis of damaged tissues but also stimulate angiogenesis and tissue cell regeneration [19]. Our findings were in accordance with Li et al. [55] that found that the exosomes derived from human umbilical cord MSCs ameliorate liver fibrosis, yet further research is still needed to determine which mediators present in EVs suspension were responsible for the improvement observed EVS group. In a recent study, it was suggested that one of the mechanisms that MSCs exosomes could ameliorate liver fibrosis is via inhibition of wnt/β-catenin signaling and preventing HSCs activation [52].

As well, it is mandatory to understand the mechanisms involved in the biological effects of EVs. In addition, the biodistribution of MSC-EVs after IV administration shows EVs uptake as fast as 3–6 h after injection in liver, spleen and lung cells [56]. Furthermore, Haga et al. [13] reported that liver, spleen, and lung from mice with fulminant hepatitis exert a higher uptake of MSC-EVs in comparison with organs from healthy mice.

Cell-free therapy, using MSC-EVs, has many advantages over cell-based therapies and may circumvent many of their limitations while retaining their therapeutic effects. Among these advantages is the fact that EVs are considered non-immunogenic, thus eliminating the risk of allogeneic immune rejection. In addition, EVs could be used as over the shelf drugs as they are easily stored and administered. Moreover, EVs could be loaded with therapeutic cargo, thus enhancing their potential therapeutic effects.

EVs-based therapeutics for the treatment of liver fibrosis has great potential, but additional challenges must be overcome. The following limitations still need to be adequately addressed: (a) Follow-up work would be necessary to determine the hepatoprotective components within the EVs and their mode of action, (b) A database of absorption, distribution, metabolism, and excretion of EVs should be established to reach the maximum therapeutic potential and well-established dosage, (c) development of a method of isolation that is highly reproducible and with increased efficiency must be defined, (d) Better targeting mechanisms should be developed to decrease off-target effects.

In conclusion, the present study revealed that EVs could reverse CCl_4-induced hepatocellular damage, ameliorate hepatic fibrosis and promote liver regeneration. Our data also indicates that the administration of MSC-EVs mimics the beneficial effects of MSC administration. Therefore, EVs present a potential therapeutic approach, not only in the treatment of liver fibrosis but also may be applied to other liver diseases while avoiding the potential risks of stem cell-based therapy. Moreover, cryopreserved EVs may be considered as a ready-to-use drug that can be injected directly and repeatedly.

Acknowledgements Acknowledgements Authors acknowledge the technical help at the Center of Excellence for Research in Regenerative Medicine Applications (CERRMA), Alexandria Faculty of Medicine. DMR and NA carried out the experimental work, Designed the experiments and co-wrote the manuscript. HMK and MWAN shared in experimental design, performed the analytical part of the study, supervised the research and revised the manuscript EAES optimized the design of experiments, supervised the research, gave conceptual advice. All authors read and approved the manuscript.

Compliance with ethical standards

Conflict of interest The authors declared no potential conflicts of interest with respect to the research, authorship, and/or publication of this article.

Ethical statement The animal studies were performed after receiving approval of the institutional review board of ethics (618/5020/2016), Faculty of medicine, University of Alexandria.

References

1. Asrani SK, Devarbhavi H, Eaton J, Kamath PS. Burden of liver diseases in the world. J Hepatol. 2019;70:151–71.
2. Hernandez-Gea V, Friedman SL. Pathogenesis of liver fibrosis. Annu Rev Pathol. 2011;6:425–56.
3. Tsolaki E, Yannaki E. Stem cell-based regenerative opportunities for the liver: state of the art and beyond. World J Gastroenterol. 2015;21:12334–50.
4. Mahla RS. Stem cells applications in regenerative medicine and disease therapeutics. Int J Cell Biol. 2016;2016:6940283.

5. Wei X, Yang X, Han ZP, Qu FF, Shao L, Shi YF. Mesenchymal stem cells: a new trend for cell therapy. Acta Pharmacol Sin. 2013;34:747–54.
6. Parekkadan B, Milwid JM. Mesenchymal stem cells as therapeutics. Annu Rev Biomed Eng. 2010;12:87–117.
7. Kim N, Cho SG. Clinical applications of mesenchymal stem cells. Korean J Intern Med. 2013;28:387–402.
8. Rani S, Ryan AE, Griffin MD, Ritter T. Mesenchymal stem cell-derived extracellular vesicles: toward cell-free therapeutic applications. Mol Ther. 2015;23:812–23.
9. Zaborowski MP, Balaj L, Breakefield XO, Lai CP. Extracellular vesicles: composition, biological relevance, and methods of study. Bioscience. 2015;65:783–97.
10. Katsuda T, Kosaka N, Takeshita F, Ochiya T. The therapeutic potential of mesenchymal stem cell-derived extracellular vesicles. Proteomics. 2013;13:1637–53.
11. Li Y, Cheng Q, Hu G, Deng T, Wang Q, Zhou J, et al. Extracellular vesicles in mesenchymal stromal cells: a novel therapeutic strategy for stroke. Exp Ther Med. 2018;15:4067–79.
12. Bruno S, Grange C, Collino F, Deregibus MC, Cantaluppi V, Biancone L, et al. Microvesicles derived from mesenchymal stem cells enhance survival in a lethal model of acute kidney injury. PLoS One. 2012;7:e33115.
13. Haga H, Yan IK, Takahashi K, Matsuda A, Patel T. Extracellular vesicles from bone marrow derived mesenchymal stem cells improve survival from lethal hepatic failure in mice. Stem Cells Transl Med. 2017;6:1262–72.
14. Gatti S, Bruno S, Deregibus MC, Sordi A, Cantaluppi V, Tetta C, et al. Microvesicles derived from human adult mesenchymal stem cells protect against ischaemia–reperfusion-induced acute and chronic kidney injury. Nephrol Dial Transplant. 2011;26:1474–83.
15. Xu R, Greening DW, Zhu HJ, Takahashi N, Simpson RJ. Extracellular vesicle isolation and characterization: toward clinical application. J Clin Invest. 2016;126:1152–62.
16. Germani G, Burroughs AK, Dhillon AP. The relationship between liver disease stage and liver fibrosis: a tangled web. Histopathology. 2010;57:773–84.
17. Ayatollahi M, Salmani MK, Geramizadeh B, Tabei SZ, Soleimani M, Sanati MH. Conditions to improve expansion of human mesenchymal stem cells based on rat samples. World J Stem Cells. 2012;26:1–8.
18. Truong NH, Nguyen NH, Le TV, Vu NB, Huynh N, Nguyen TV, et al. Comparison of the treatment efficiency of bone marrow-derived mesenchymal stem cell transplantation via tail and portal veins in CCl4-induced mouse liver fibrosis. Stem Cells Int. 2016;2016:5720413.
19. Motawi TM, Atta HM, Sadik NA, Azzam M. The therapeutic effects of bone marrow-derived mesenchymal stem cells and simvastatin in a rat model of liver fibrosis. Cell Biochem Biophys. 2014;68:111–25.
20. Kurtz A. Mesenchymal stem cell delivery routes and fate. Int J Stem Cells. 2008;1:1–7.
21. Pochampally R. Colony forming unit assays for MSCs. Methods Mol Biol. 2008;449:83–91.
22. Sun S, Guo Z, Xiao X, Liu B, Liu X, Tang PH, et al. Isolation of mouse marrow mesenchymal progenitors by a novel and reliable method. Stem Cells. 2003;21:527–35.
23. Bayati V, Hashemitabar M, Gazor R, Nejatbakhsh R, Bijannejad D. Expression of surface markers and myogenic potential of rat bone marrow- and adipose-derived stem cells: a comparative study. Anat Cell Biol. 2013;46:113–21.
24. Hayes O, Ramos B, Rodriguez LL, Aguilar A, Badia T, Castro FO. Cell confluency is as efficient as serum starvation for inducing arrest in the G0/G1 phase of the cell cycle in granulosa and fibroblast cells of cattle. Anim Reprod Sci. 2005;87:181–92.
25. Théry C, Amigorena S, Raposo G, Clayton A. Isolation and characterization of exosomes from cell culture supernatants and biological fluids. Curr Protoc Cell Biol. 2006;Chapter3:Unit3.22.
26. Gudbergsson JM, Johnsen KB, Skov MN, Duroux M. Systematic review of factors influencing extracellular vesicle yield from cell cultures. Cytotechnology. 2016;68:579–92.
27. Rupert DLM, Claudio V, Lässer C, Bally M. Methods for the physical characterization and quantification of extracellular vesicles in biological samples. Biochim Biophys Acta Gen Subj. 2017;1861:3164–79.
28. Phinney DG, Pittenger MF. Concise review: MSC-derived exosomes for cell-free therapy. Stem Cells. 2017;35:851–8.
29. Bian S, Zhang L, Duan L, Wang X, Min Y, Yu H. Extracellular vesicles derived from human bone marrow mesenchymal stem cells promote angiogenesis in a rat myocardial infarction model. J Mol Med (Berl). 2014;92:387–97.
30. Teng X, Chen L, Chen W, Yang J, Yang Z, Shen Z. Mesenchymal stem cell-derived exosomes improve the microenvironment of infarcted myocardium contributing to angiogenesis and anti-inflammation. Cell Physiol Biochem. 2015;37:2415–24.
31. Xin H, Li Y, Cui Y, Yang JJ, Zhang ZG, Chopp M. Systemic administration of exosomes released from mesenchymal stromal cells promote functional recovery and neurovascular plasticity after stroke in rats. J Cereb Blood Flow Metab. 2013;33:1711–5.
32. Hartjes TA, Mytnyk S, Jenster GW, van Steijn V, van Royen ME. Extracellular vesicle quantification and characterization: common methods and emerging approaches. Bioengineering (Basel). 2019;6:E7.
33. Wang M, Zhang X, Xiong XI,, Yang Z, Li P, Wang J, et al. Bone marrow mesenchymal stem cells reverse liver damage in a carbon tetrachloride-induced mouse model of chronic liver injury. In Vivo. 2016;30:187–93.
34. Edinger AL, Thompson CB. Death by design: apoptosis, necrosis and autophagy. Curr Opin Cell Biol. 2004;16:663–9.
35. Zhao DC, Lei JX, Chen R, Yu WH, Zhang XM, Li SN, et al. Bone marrow-derived mesenchymal stem cells protect against experimental liver fibrosis in rats. World J Gastroenterol. 2005;11:3431–40.
36. Cai Y, Gong LK, Qi XM, Li Xh, Ren J. Apoptosis initiated by carbon tetrachloride in mitochondria of rat primary cultured hepatocytes. Acta Pharmacol Sin. 2005;26:969–75.
37. Scholten D, Weiskirchen R. Questioning the challenging role of epithelial-to-mesenchymal transition in liver injury. Hepatology. 2011;53:1048–51.
38. Marzano C, Cazals-Hatem D, Rautou PE, Valla DC. The significance of nonobstructive sinusoidal dilatation of the liver: impaired portal perfusion or inflammatory reaction syndrome. Hepatology. 2015;62:956–63.
39. Luckey SW, Petersen DR. Activation of Kupffer cells during the course of carbon tetrachloride-induced liver injury and fibrosis in rats. Exp Mol Pathol. 2001;71:226–40.
40. Sato K, Marzioni M, Meng F, Francis H, Glaser S, Alpini G. Ductular reaction in liver diseases: pathological mechanisms and translational significances. Hepatology. 2019;69:420–30.
41. Kumar V, Abbas AK, Aster JC. Robbins basic pathology. 9th ed. Philadelphia: Saunders; 2012. p. 1–30.
42. Fausto N, Campbell JS. The role of hepatocytes and oval cells in liver regeneration and repopulation. Mech Dev. 2003;120:117–30.
43. Hamamoto H, Gorman JH 3rd, Ryan LP, Hinmon R, Martens TP, Schuster MD, et al. Allogeneic mesenchymal precursor cell therapy to limit remodeling after myocardial infarction: the effect of cell dosage. Ann Thorac Surg. 2009;87:794–801.
44. Hashemi SM, Ghods S, Kolodgie FD, Parcham-Azad K, Keane M, Hamamdzic D, et al. A placebo controlled, dose-ranging, safety study of allogenic mesenchymal stem cells injected by

endomyocardial delivery after an acute myocardial infarction. Eur Heart J. 2008;29:251–9.
45. Yamanaka N, Okamoto E, Kawamura E, Kato T, Oriyama T, Fujimoto J, et al. Dynamics of normal and injured human liver regeneration after hepatectomy as assessed on the basis of computed tomography and liver function. Hepatology. 1993;18:79–85.
46. Tsuchida T, Friedman SL. Mechanisms of hepatic stellate cell activation. Nat Rev Gastroenterol Hepatol. 2017;14:397–411.
47. Carpino G, Morini S, Ginanni Corradini S, Franchitto A, Merli M, Siciliano M, et al. Alpha-SMA expression in hepatic stellate cells and quantitative analysis of hepatic fibrosis in cirrhosis and in recurrent chronic hepatitis after liver transplantation. Dig Liver Dis. 2005;37:349–56.
48. Ahmed SK, Mohammed SA, Khalaf G, Fikry H. Role of bone marrow mesenchymal stem cells in the treatment of CCL4 induced liver fibrosis in albino rats: a histological and immunohistochemical study. Int J Stem Cells. 2014;7:87–97.
49. Brenner DA. Reversibility of liver fibrosis. Gastroenterol Hepatol (N Y). 2013;9:737–9.
50. Nargesi AA, Lerman LO, Eirin A. Mesenchymal stem cell-derived extracellular vesicles for renal repair. Curr Gene Ther. 2017;17:29–42.
51. Usunier B, Benderitter M, Tamarat R, Chapel A. Management of fibrosis: the mesenchymal stromal cells breakthrough. Stem Cells Int. 2014;2014:340257.
52. Rong X, Liu J, Yao X, Jiang T, Wang Y, Xie F. Human bone marrow mesenchymal stem cells-derived exosomes alleviate liver fibrosis through the Wnt/β-catenin pathway. Stem Cell Res Ther. 2019;10:98.
53. Hu C, Zhao L, Duan J, Li L. Strategies to improve the efficiency of mesenchymal stem cell transplantation for reversal of liver fibrosis. J Cell Mol Med. 2019;23:1657–70.
54. van Poll D, Parekkadan B, Cho CH, Berthiaume F, Nahmias Y, Tilles AW, et al. Mesenchymal stem cell-derived molecules directly modulate hepatocellular death and regeneration in vitro and in vivo. Hepatology. 2008;47:1634–43.
55. Li T, Yan Y, Wang B, Qian H, Zhang X, Shen L, et al. Exosomes derived from human umbilical cord mesenchymal stem cells alleviate liver fibrosis. Stem Cells Dev. 2013;22:845–54.
56. Fiore EJ, Domínguez LM, Bayo J, García MG, Mazzolini GD. Taking advantage of the potential of mesenchymal stromal cells in liver regeneration: cells and extracellular vesicles as therapeutic strategies. World J Gastroenterol. 2018;24:2427–40.